

Nonlinear Behavior of a Discrete-PWM Controlled Buck Converter and its Influence on the Power Spectrum

Jeroen Tant, *Student Member, IEEE*, Jan Verwecken, *Student Member, IEEE*, and Johan Driesen, *Member, IEEE*

Abstract—In this paper, the nonlinear behavior of a practical discrete PWM controlled buck converter is analyzed. The converter is modeled as a discrete-time piecewise smooth iterative map. A bifurcation diagram is generated with numerical continuation software. High-periodic, quasiperiodic and chaotic equilibrium solutions are found. Characteristic power spectrum properties for each type of equilibrium solution are discussed. The resulting power spectrum profiles can be used to identify the type of the equilibrium solution with a spectrum analyzer. Simulation results are validated with measurements on a buck converter platform, confirming the capability of the idealized model to predict nonlinear behavior.

I. INTRODUCTION

Nonlinear phenomena, bifurcations and chaos have been observed in various types of switched power electronic converters [1], [2], including peak-current mode [3], pulse width modulation (PWM) [4] and sliding mode [5] controlled DC/DC converters. Most of these converters are controlled by an analog circuit. A real world buck converter with a practical digital PWM control system is investigated in this paper.

A qualitative nonlinear analysis gives insights for the design and analysis of control systems for power electronic converters. Usually, the switching frequency f_s is a design parameter for the output filters. The operation of some converters depends heavily on the assumption that the equilibrium solution is periodic with frequency f_s . High-periodic, quasiperiodic or chaotic equilibrium solutions introduce subharmonic components in the power spectrum and affect the signal quality significantly, reducing the effectiveness of the output filter. Even when a converter is designed for a periodic working point, parameter drift could bring the converter into an undesired operating region with subharmonic content.

In [6], some applications of chaos in power electronic converters are considered. Typically, chaos gives rise to a broad power spectrum and can help for the design of high-frequency converters to improve the electromagnetic compatibility [7]. On the other hand, there is always a trade-off between the broad spectrum and signal quality.

For the aforementioned reasons, it is important to know the parameter range in which different types of equilibrium solutions occur. This can be summarized in a bifurcation diagram. A bifurcation diagram is a general tool for nonlinear

analysis and shows the equilibrium solutions as a function of a parameter [8].

In order to generate a bifurcation diagram, the derivation of a discrete iterative map [9] is needed. For switched power electronic circuits, this map is usually piecewise smooth. In literature, the bifurcation diagram for this piecewise smooth map is created with a brute force method. This is done by simulating the iterative map for many iterations until an equilibrium state is reached, and by repeating this for multiple parameter values. In this work, the bifurcation diagram is calculated numerically by means of numerical continuation software. The influence of nonlinear equilibrium solutions on the power spectrum is investigated.

As the switches and components in the model are assumed to be ideal, the question arises whether this model is able to accurately describe the real converter dynamics. This is confirmed with measurement results obtained from an experimental setup.

II. MATHEMATICAL CONCEPTS

A. Piecewise smooth iterative map

A continuous trajectory in state space can be sampled with the switching frequency f_s , resulting in a discrete state vector \mathbf{x}_k . An iterative map can be defined, giving the discrete state variables for the next period as a function of the current discrete state variables. In this paper, the resulting iterative map is piecewise smooth. In a piecewise smooth map, the state space is partitioned in n_r different regions \mathcal{R}_i ($i = 1 \dots n_r$). In each region, a different smooth map \mathbf{F}_i is valid (Figure 1a) [10].

$$\mathbf{x}_{k+1} = \mathbf{F}_i(\mathbf{x}_k) \quad \mathbf{x}_k \in \mathcal{R}_i \quad (1)$$

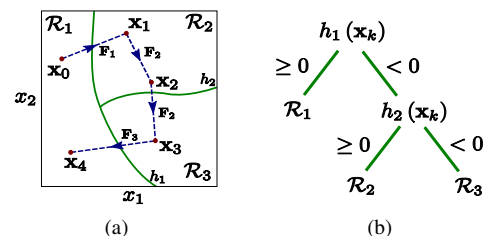


Fig. 1: Example of a piecewise smooth map: state space partitioning (a) and its associated tree structure (b).

$n_r - 1$ border equations h_j . Figure 1b shows that the current state vector \mathbf{x}_k can be associated with the current region by using a tree structure of border equations. A state \mathbf{x}_k is required to comply with a number of inequalities in order to belong to a region \mathcal{R}_i . The inequalities can be gathered in a system of inequalities \mathbf{g}_i :

$$\mathbf{g}_i(\mathbf{x}_k) > \mathbf{0} \Rightarrow \mathbf{x}_k \in \mathcal{R}_i. \quad (2)$$

The sequence of region indices r_k along the path followed by the state vector \mathbf{x}_k is called the symbolic sequence [10]. The symbolic sequence for the example of Figure 1a is given as:

$$\{r_0, r_1, r_2, r_3, r_4, \dots\} = \{1, 2, 2, 3, 1, \dots\}. \quad (3)$$

B. Lyapunov exponents

A trajectory starting in an infinitesimally small perturbed initial point $\mathbf{x}_0 + \delta\mathbf{x}_0$ can diverge or converge to the original trajectory starting in \mathbf{x}_0 . The deviation after n iterations can be written as

$$\delta\mathbf{x}_n \approx \mathbf{J}_{r_n}(\mathbf{x}_n) \cdot \dots \cdot \mathbf{J}_{r_1}(\mathbf{x}_1) \cdot \mathbf{J}_{r_0}(\mathbf{x}_0) \cdot \delta\mathbf{x}_0 = \mathbf{J}_n \cdot \delta\mathbf{x}_0 \quad (4)$$

where \mathbf{J}_{r_k} is the Jacobian of the iterative map \mathbf{F}_{r_k} .

$$\mathbf{J}_{r_k}(\mathbf{x}_k) = \left. \frac{\partial \mathbf{F}_{r_k}(\mathbf{x})}{\partial \mathbf{x}} \right|_{\mathbf{x}=\mathbf{x}_k} \quad (5)$$

The singular values $\sigma_j(n)$ (with $j = 1 \dots n_d$) of \mathbf{J}_n are indicators for the growth of the deviation in the corresponding direction. The Lyapunov exponents λ_j for this trajectory are defined as [11]:

$$\lambda_j = \lim_{n \rightarrow +\infty} \left(\frac{1}{n} \ln |\sigma_j(n)| \right). \quad (6)$$

The trajectory will converge to the original trajectory when all Lyapunov exponents are negative. The trajectory will diverge when one of the Lyapunov exponents is positive.

C. Equilibrium solutions

1) *1-periodic solutions*: A 1-periodic equilibrium solution $\tilde{\mathbf{x}}_0$ is mapped onto itself:

$$\mathbf{F}(\tilde{\mathbf{x}}_0) = \tilde{\mathbf{x}}_0. \quad (7)$$

This equilibrium solution is stable when all eigenvalues of the Jacobian $\mathbf{J}_{\tilde{r}}(\tilde{\mathbf{x}})$ lay within the unit circle and then all Lyapunov exponents are negative.

The trajectory in continuous-time domain is periodic with period $T_s = 1/f_s$. The power spectrum consists of a DC-component, a fundamental component at the switching frequency f_s and harmonic components at integer multiples of f_s .

2) *n_p -periodic solutions*: An n_p -periodic equilibrium point $\tilde{\mathbf{x}}_0$ is mapped onto itself after n_p iterations.

$$\tilde{\mathbf{x}}_0 = \mathbf{F}_{\tilde{r}_{n_p-1}} \circ \dots \circ \mathbf{F}_{\tilde{r}_1} \circ \mathbf{F}_{\tilde{r}_0}(\tilde{\mathbf{x}}_0) \quad (8)$$

The continuous trajectory is periodic with period $n_p T_s$ and its power spectrum contains components at integer multiples of $\frac{1}{n_p} f_s$. Thus, there are subharmonic components with frequencies below the switching frequency f_s .

3) *Quasiperiodic solutions*: When a stable quasiperiodic equilibrium solution is present, nearby iteration points are attracted to a closed invariant loop. Points on the invariant loop are always mapped back onto the loop but never onto the same point again, i.e. the solution is not periodic. One of the Lyapunov exponents will evaluate exactly zero.

In continuous-time domain, an additional rotation frequency f_r next to the fundamental switching frequency f_s is observed and the ratio $\frac{f_r}{f_s}$ is irrational [10]. The power spectrum is filled with components at integer combinations of the frequencies f_s and f_r [12].

4) *Chaos*: A chaotic attractor is an invariant set with a fractal dimension. At least one of the Lyapunov exponents is greater than zero, thus perturbed iterations will diverge and this implies a great sensitivity to variations on the initial conditions. The continuous trajectory is not periodic and not quasiperiodic, has a random character and is hard to predict because of the sensitivity to the initial conditions. Nevertheless, the trajectory is deterministic [8]. As the trajectory is aperiodic, the power spectrum will be continuous.

III. PWM-CONTROLLED BUCK CONVERTER

A. Experimental setup

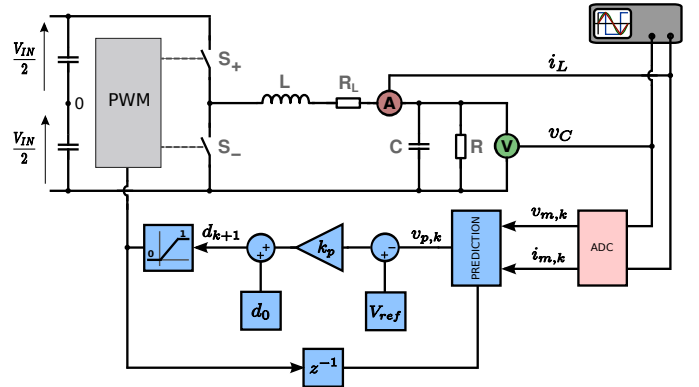


Fig. 2: Experimental setup for the PWM-controlled buck converter.

An experimental setup was built around the Triphase Smart Inverter Target Platform [13]. The circuit in Figure 2 shows how one inverter leg is used to create a buck converter. The parameter values used for all simulations and measurements are summarized in Table I. The inverter leg is controlled by a symmetrical digital PWM controller with fixed switching period T_s . For each switching period k , a PWM duty cycle d_k is determined by the digital control circuit. The saturation block in the diagram clips the actual duty cycle \hat{d}_k between zero and one.

$$\hat{d}_k = \begin{cases} 0 & d_k < 0 \\ d_k & 0 \leq d_k < 1 \\ 1 & d_k \geq 1 \end{cases} \quad (9)$$

The switching period events and corresponding notations are summarized in Figure 3. At the beginning of each switching period, the inductor current i_L is instantly sampled with a

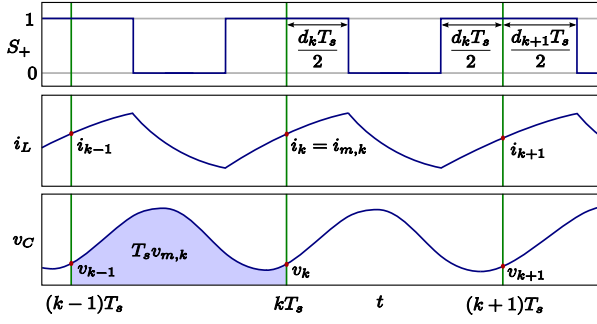


Fig. 3: Timing diagram showing the events in one switching period.

TABLE I: Parameter values used in the experimental setup.

R	L	R_L	C	V_{ref}	V_{in}	k_p	T_s	d_0
25.5	10	0.4	9.9	230	287	0.002 → 0.2	100	0.5
[Ω]	[mH]	[Ω]	[μF]	[V]	[V]	[–]	[μs]	[–]

Successive Approximation Register A/D converter, resulting in a measured value $i_{m,k}$.

$$i_{m,k} = i_k = i_L(kT_s) \quad (10)$$

The capacitor voltage v_C is sampled with a Sigma-Delta A/D converter. The measured value $v_{m,k}$ is an approximation for the mean voltage value in the previous switching period:

$$v_k = v_C(kT_s) \quad v_{m,k} = \frac{1}{T_s} \int_{(k-1)T_s}^{kT_s} v_C(t) dt. \quad (11)$$

There is a delay of one sample in the digital control system loop because the measured values $i_{m,k}$ and $v_{m,k}$ at the start of the current switching period are used to determine the duty cycle d_{k+1} for the following period. Therefore, current and voltage values $i_{p,k}$ and $v_{p,k}$ for the next period are predicted with a linearized model.

$$\begin{bmatrix} i_{p,k} \\ v_{p,k} \end{bmatrix} = M \begin{bmatrix} i_{m,k} \\ v_{m,k} \end{bmatrix} + N \hat{d}_k \quad N = \int_0^{T_s} e^{A_p t} \mathbf{b}_p dt \quad (12)$$

$$M = e^{A_p T_s} \quad A_p = \begin{bmatrix} -\frac{R_L}{L} & \frac{1}{L} \\ \frac{1}{C} & -\frac{1}{RC} \end{bmatrix} \quad \mathbf{b}_p = \begin{bmatrix} \frac{V_{\text{in}}}{L} \\ 0 \\ 0 \end{bmatrix} \quad (13)$$

The proportional control law is implemented as follows:

$$d_{k+1} = k_p (V_{\text{ref}} - v_{p,k}) + d_0. \quad (14)$$

B. Continuous switch state equations

Two valid switch states s are distinguished: one with S^+ closed and S^- open ($s = 1$) and one with S^+ open and S^- closed ($s = 2$). For each switch state, the dynamics can be described with a continuous state space model with state vector $\mathbf{x} = [i_L \ v_C \ v_m]^T$. The state variables are the inductor current i_L and capacitor voltage v_C . The variable v_m is needed to calculate the A/D converter integral in equation (11). The state

space model can be written as a system of linear differential equations.

$$\dot{\mathbf{x}} = A\mathbf{x} + \mathbf{b}_s \quad s \in \{1, 2\} \quad (15)$$

$$A = \begin{bmatrix} -\frac{R_L}{L} & -\frac{1}{L} & 0 \\ \frac{1}{C} & -\frac{1}{RC} & 0 \\ 0 & \frac{1}{T_s} & 0 \end{bmatrix} \quad \mathbf{b}_1 = \begin{bmatrix} \frac{V_{\text{in}}}{L} \\ 0 \\ 0 \end{bmatrix} \quad \mathbf{b}_2 = \begin{bmatrix} 0 \\ 0 \\ 0 \end{bmatrix} \quad (16)$$

The solution for this system of linear differential equations is given as

$$\mathbf{x}(t) = \Psi_s(\mathbf{x}_0, t) = e^{At} \mathbf{x}_0 + \int_0^t e^{A\tau} \mathbf{b}_s d\tau. \quad (17)$$

C. Piecewise smooth map

The discrete state vector $\mathbf{x}_k = [i_k \ v_k \ v_{m,k}]^T$ can be augmented with an extra state for the duty cycle d_k : $\hat{\mathbf{x}}_k = [i_k \ v_k \ v_{m,k} \ d_k]^T$. The borders $d_k = 0$ and $d_k = 1$ partition the state space in three regions as shown in the tree structure in Figure 4.

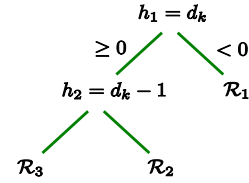


Fig. 4: Tree structure defining the three state space partitions.

For the ease of notation a reset matrix R and a prediction matrix \hat{M} are defined:

$$R = \begin{bmatrix} 1 & 0 & 0 \\ 0 & 1 & 0 \\ 0 & 0 & 0 \end{bmatrix} \quad \hat{M} = M \begin{bmatrix} 1 & 0 & 0 \\ 0 & 0 & 1 \end{bmatrix} \quad (18)$$

The reset matrix is used to reset the integral in equation (11) at the start of each switching period. The piecewise smooth map for the discrete PWM controlled buck converter in Figure 2 is given as:

$$\hat{\mathbf{x}}_{k+1} = \begin{cases} \begin{bmatrix} \Psi_2(R\mathbf{x}_k, T_s) \\ k_p (V_{\text{ref}} - [0 \ 1] (\hat{M}\mathbf{x}_k + N \cdot 0)) + d_0 \end{bmatrix} & \hat{\mathbf{x}}_k \in \mathcal{R}_1 \\ \begin{bmatrix} \Psi_1 \left(\Psi_2 \left(\Psi_1 \left(R\mathbf{x}_k, \frac{d_k T_s}{2} \right), (1-d_k)T_s \right), \frac{d_k T_s}{2} \right) \\ k_p (V_{\text{ref}} - [0 \ 1] (\hat{M}\mathbf{x}_k + N d_k)) + d_0 \end{bmatrix} & \hat{\mathbf{x}}_k \in \mathcal{R}_2 \\ \begin{bmatrix} \Psi_1(R\mathbf{x}_k, T_s) \\ k_p (V_{\text{ref}} - [0 \ 1] (\hat{M}\mathbf{x}_k + N \cdot 1)) + d_0 \end{bmatrix} & \hat{\mathbf{x}}_k \in \mathcal{R}_3. \end{cases} \quad (19)$$

IV. SIMULATION RESULTS

A. Bifurcation diagram

The proportional control parameter k_p is varied as a bifurcation parameter and a bifurcation diagram is generated. The projection of the diagram in the $d_k - k_p$ plane is given in Figure 5a. Branches with periodic solutions are computed

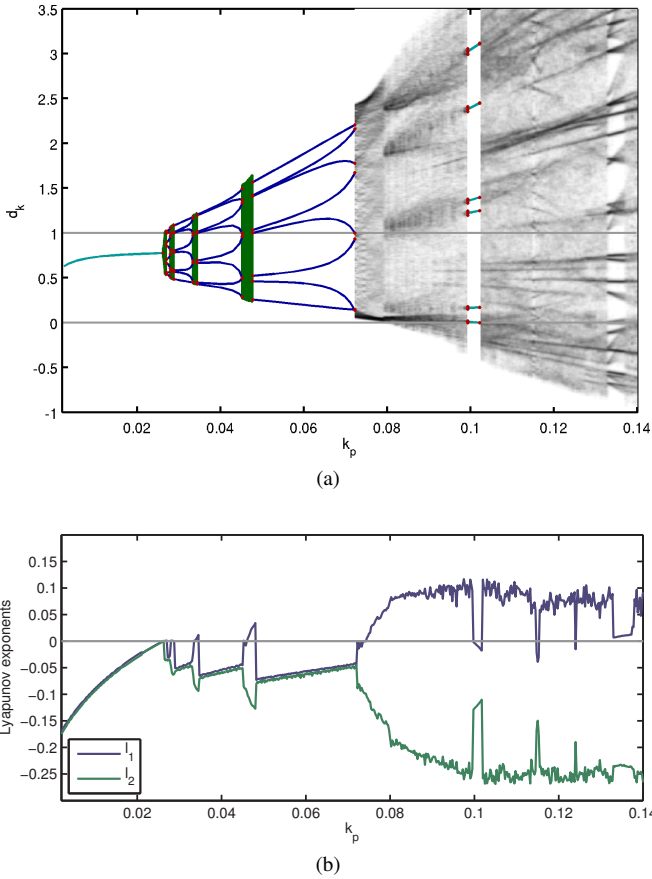


Fig. 5: Bifurcation diagram (a) and Lyapunov spectrum (b) for the discrete PWM controlled *buck converter*.

numerically with CL_MATCONTM [14], a continuation toolbox for MATLAB[®]. This software is designed for smooth maps and does not work for piecewise smooth maps out of the box. Therefore, the method described in [15] is used to apply CL_MATCONTM to piecewise smooth maps. For quasiperiodic solutions, the projection of the invariant loop is drawn on the diagram. In chaotic regime, the density of the iteration points is plotted.

Subsequently, the Lyapunov exponents are plotted in Figure 5b as a function of the bifurcation parameter k_p . The Lyapunov exponents are calculated with the method described in [16]. Only the two largest exponents are shown on the figure.

The bifurcation diagram is analyzed with time domain simulations at four bifurcation parameter values:

1) $k_p = 0.015$: The equilibrium solution is 1-periodic and stable, all Lyapunov exponents are negative. The 1-periodic inductor current waveform is shown in Figure 6a. The 1-periodic branch in the bifurcation diagram ends in a Neimark-Sacker bifurcation point. At this bifurcation point, the equilibrium solution changes from a 1-periodic to a quasiperiodic solution.

2) $k_p = 0.027$: The solution is quasiperiodic and one of the Lyapunov exponents is zero. The waveform is shown in Figure 6b.

3) $k_p = 0.036$: For this value, the equilibrium solution is n_p -periodic ($n_p = 8$, Figure 6c). The borders $d_k = 0$ and

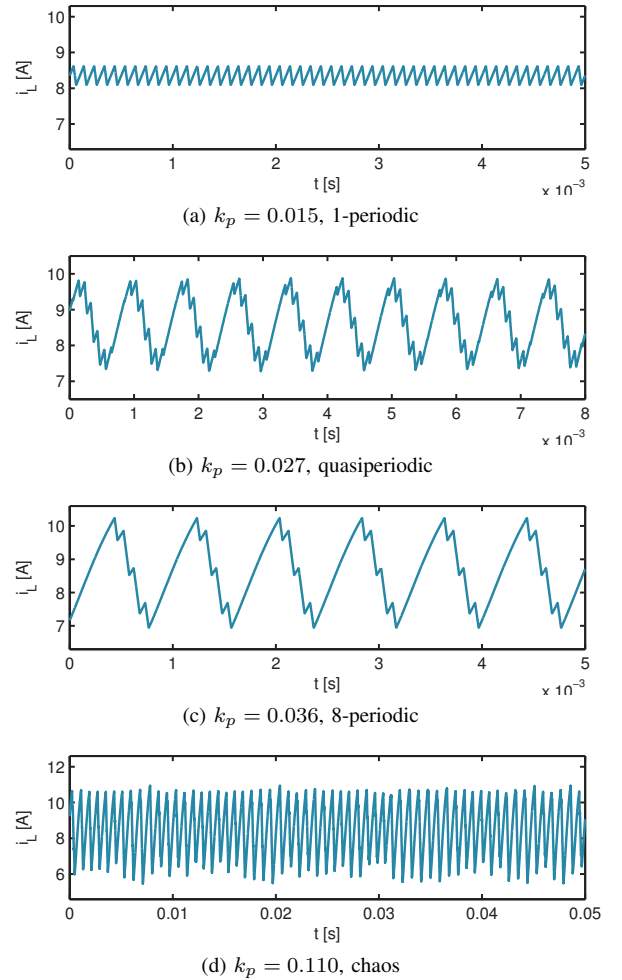


Fig. 6: Inductor current waveforms for four different positions on the bifurcation diagram.

$d_k = 1$ are drawn onto the diagram. The 8-periodic equilibrium branches stop when one of the borders is reached. At these points, one of the border equations in system (2) evaluates exactly zero. These are border collision bifurcation points [10].

4) $k_p = 0.110$: The solution is chaotic, as shown in Figure 6d. One of the Lyapunov exponents is larger than zero. When the bifurcation parameter is varied from left to right in Figure 5a, the bifurcation diagram transverse various zones with periodic and quasiperiodic equilibrium solutions, until a parameter range with chaos is reached. This is called a quasiperiodic route to chaos [2]. In the parameter range with chaos, some periodic windows occur at the locations where all Lyapunov exponents are negative.

B. Influence on the power spectrum

The power spectra of the inductor current waveforms in Figure 6 are displayed in Figure 7. In Figure 7a, the normal 1-periodic operation is shown. The DC component, the switching frequency f_s at 10 kHz and a second harmonic component at 20 kHz can be identified. These components are also visible in the quasiperiodic spectrum in Figure 7b. Additionally, an extra rotation frequency f_r appears in the spectrum at approximately 1256 Hz. The ratio $\frac{f_r}{f_s}$ is irrational. The mirror components

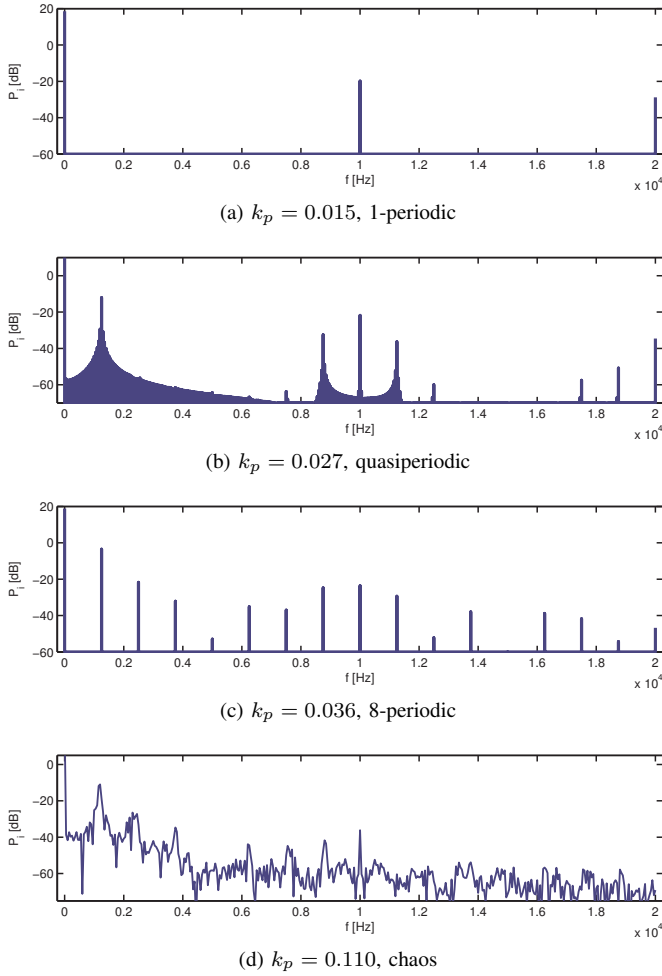


Fig. 7: Simulated power spectra of the inductor current i_L .

$f_s - f_r$ and $f_s + f_r$ are clearly visible and the spectrum is filled with integer combinations of f_s and f_r .

In the 8-periodic operation mode (Figure 7c), the spectrum contains a first subharmonic component at $f_{1/8} = 1250$ Hz. The ratio $\frac{f_{1/8}}{f_s} = \frac{1}{8}$ is rational and the spectrum is filled with integer multiples of $f_{1/8}$. The spectrum of operation in chaos is displayed in Figure 7d. The spectrum is continuous and there is a lot of subharmonic content.

V. EXPERIMENTAL VALIDATION

The previous simulation results are based on an idealized model. Non-ideal switches, dead time, quantization, noise and parasitic effects were not taken into account. Three validation measurements are carried out to test the capability of the idealized model to predict nonlinear behavior in real world applications.

A. Continuous-time domain

The inductor current and capacitor voltage are measured using a digital sampling oscilloscope and plotted in the $i_L - v_C$ phase plane. Measurement results for the quasiperiodic, 8-periodic and chaotic solutions are given in the right column of Figure 8 and correspond well with the simulation results in

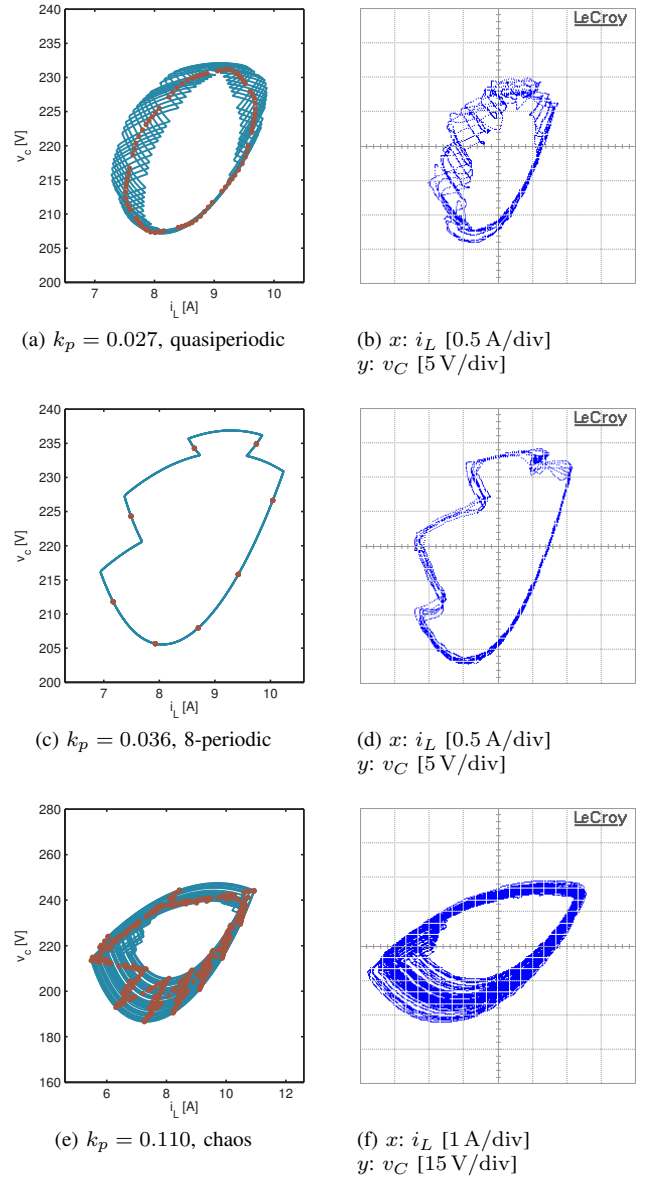


Fig. 8: Phase trajectory, comparison between simulation (left column) and measurement (right column) results.

the left column. In the simulation figures, a dot is plotted at each time instant kT_s .

B. Frequency domain

Additionally, the power spectrum of the inductor current is measured with a spectrum analyzer. Results are shown in Figure 9 and match with the simulation results in Figure 7.

C. Discrete-time domain

Finally, 50000 iteration points $(i_{m,k}, v_{m,k})$, sampled by the digital control system, are plotted in Figure 10. The quasiperiodic invariant loop is clearly visible in Figures 10a and 10b. The 8 equilibrium points of the 8-periodic solution can be distinguished in Figures 10c and 10d, with Gaussian noise around the measured results. The chaotic attractor with fractal dimension is shown in Figures 10e and 10f.

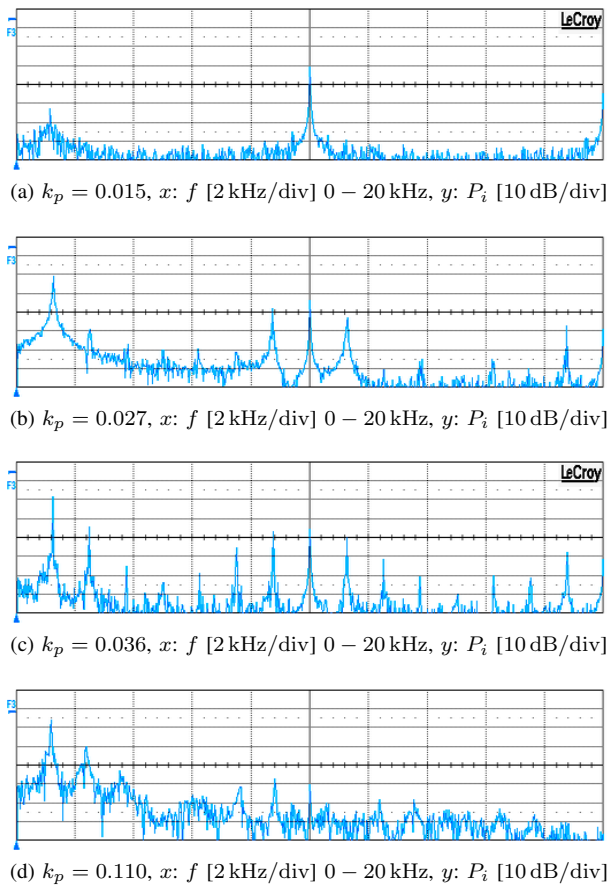


Fig. 9: Measured power spectra of the inductor current i_L .

VI. CONCLUSIONS

A quasiperiodic route to chaos is found in a buck converter with discrete PWM controller and a bifurcation diagram is generated. Simulations conducted with an idealized model are confirmed with measurement results. All observed nonlinear effects can be explained by means of the ideal model. The nonlinear solutions can be distinguished by their specific subharmonic content in the power spectrum. Using these characteristics, it is possible to identify nonlinear solutions with the aid of a spectrum analyzer. Vice versa, the equilibrium solutions in the bifurcation diagram can be used to predict the shape of the power spectrum.

REFERENCES

- [1] S. Banerjee and G. C. Verghese, Eds., *Nonlinear Phenomena in Power Electronics: attractors, bifurcations, chaos, and nonlinear control*. Wiley-IEEE Press, 2001.
- [2] C. K. Tse, *Complex Behavior of Switching Power Converters (Power Electronics and Applications Series)*. CRC, 2003.
- [3] J. Deane, "Chaos in a current-mode controlled boost dc-dc converter," *Circuits and Systems I: Fundamental Theory and Applications, IEEE Transactions on*, vol. 39, no. 8, pp. 680–683, Aug 1992.
- [4] S. K. Maumder, A. H. Nayfeh, and D. Boroyevich, "Theoretical and experimental investigation of the fast- and slow-scale instabilities of a dc-dc converter," *IEEE Transactions on Power Electronics*, vol. 16, no. 2, p. 201, 2001.
- [5] J. Calvente, "Subharmonics, bifurcations and chaos in a sliding-mode controlled boost switching regulator," in *1996 IEEE International Symposium on Circuits and Systems Connecting the World ISCAS 96*, vol. 1, 1996, p. 573.

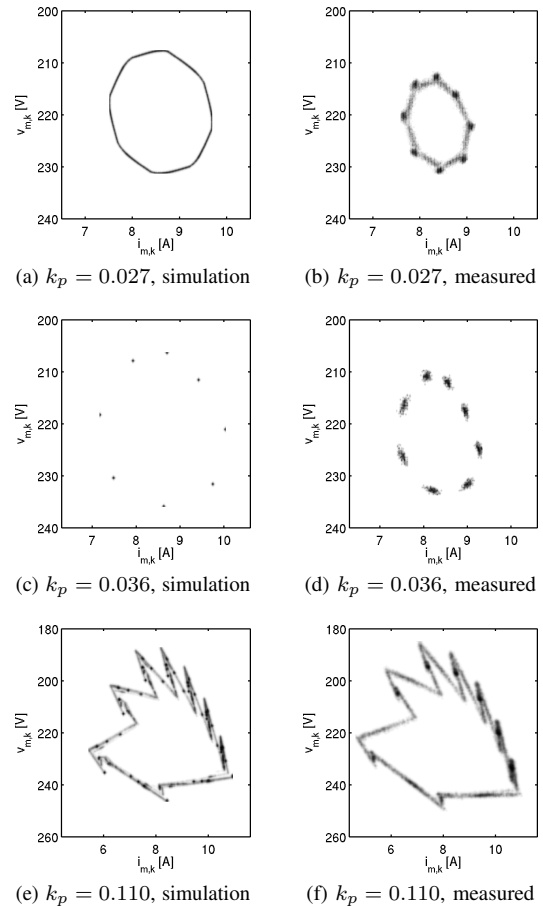


Fig. 10: Discrete iteration points in the $i_{m,k} - v_{m,k}$ plane, simulation vs. measurement.

- [6] D. Hamill, J. Deane, and P. Aston, "Some applications of chaos in power converters," in *Update on New Power Electronic Techniques (Digest No: 1997/091), IEE Colloquium on*, May 1997, pp. 5/1–5/5.
- [7] J. Deane, P. Ashwin, D. Hamill, and D. Jefferies, "Calculation of the periodic spectral components in a chaotic dc-dc converter," *Circuits and Systems I: Fundamental Theory and Applications, IEEE Transactions on*, vol. 46, no. 11, pp. 1313–1319, Nov 1999.
- [8] S. H. Strogatz, *Nonlinear Dynamics And Chaos: With Applications To Physics, Biology, Chemistry, And Engineering (Studies in nonlinearity)*. Westview Press, 2001.
- [9] M. di Bernardo, "Discrete-time maps for the analysis of bifurcations and chaos in dc/dc converters," *IEEE Transactions on Circuits and Systems I Fundamental Theory and Applications*, vol. 47, no. 2, p. 130, 2000.
- [10] —, *Piecewise-smooth Dynamical Systems: Theory and Applications*. Springer, 2007.
- [11] P. Cvitanović, R. Artuso, R. Mainieri, G. Tanner, and G. Vattay, "Chapter: averaging," in *Chaos: Classical and Quantum*. Niels Bohr Institute, Copenhagen, 2008, ch. 15. [Online]. Available: <http://ChaosBook.org/version12>
- [12] F. Schilder, W. Vogt, S. Schreiber, and H. M. Osinga, "Fourier methods for quasi-periodic oscillations," *International journal for numerical methods in engineering*, vol. 67, no. 5, pp. 629–671, 2006.
- [13] Triphase. [Online]. Available: <http://www.triphase.com>
- [14] W. Govaerts, Y. A. Kuznetsov, R. Khoshshar Ghaziani, and H. G. E. Meijer, *CL_MATCONTM: A toolbox for continuation and bifurcation of cycles of maps*, march 2008. [Online]. Available: <http://sourceforge.net/projects/matcont/>
- [15] J. Tant, "Niet-lineaire dynamica in vermogenelektronische omvormers," Master's thesis, Katholieke Universiteit Leuven, 2009.
- [16] H. F. von Bremen, F. E. Udawadia, and W. Proskurowski, "An efficient QR based method for the computation of lyapunov exponents," *Physica D: Nonlinear Phenomena*, vol. 101, no. 1-2, pp. 1 – 16, 1997.